AIAA JOURNAL
Vol. 30, No. 6, June 1992

Predictions of Turbulent Mixing in Axisymmetric Compressible Shear Layers

K. Viswanathan* and P. J. Morris†
Pennsylvania State University, University Park, Pennsylvania 16802

Models are described for the turbulent mixing of compressible, axisymmetric shear layers. The models assume that the mixing process is dominated by large-scale coherent structures. These large-scale structures are described locally as linear instability waves. Calculations are made for the development of the axisymmetric shear layer as a function of freestream Mach numbers and velocity and density ratios. The predictions for the axisymmetric shear layer are compared with both experimental measurements and predictions for a plane shear layer. The effects of the initial thickness of the shear layer and the initial amplitudes of the large-scale structures on the growth of the shear layer are examined. The effect of the description of the mean velocity profile is considered.

I. Introduction

IT is now acknowledged generally that the mixing process in low-speed free shear layers is dominated by large-scale structures. Turbulent mixing is observed to consist of an engulfment process that captures large quantities of unmixed fluid and transports them across the shear layer. Many studies using flow visualization,[1] conditional sampling,[2] and controlled excitation techniques[3,4] have led to a better understanding of the structure and role of these large-scale structures. However, few turbulence models have been developed that make use of the importance of these structures. The present model assumes that large-scale structures continue to control the mixing process at high speeds, though the nature of the structures may change with the operating conditions. Lepicovsky et al.[5] showed that both helical and axisymmetric structures are present in supersonic jets. Papamoschou and Roshko[6] have observed large-scale structures in supersonic shear layers, though their degree of organization appears to be less than that observed at low speeds.

In the present model, the large-scale structures are modeled locally as linear instability waves. There are many experimental studies in both jets and shear layers that demonstrate that when the large-scale structures are phase locked by external excitation, to permit their characteristics to be observed more easily, their local distributions of amplitude and phase are modeled remarkably well by a local, linear, inviscid stability analysis. Examples may be found in Gaster et al.[3] and Petersen and Samet.[4] In addition, other analyses based on the modeling of the large-scale structures in jets and shear layers as instability waves have been successful in the description of the noise radiation from supersonic jets (Refs. 7 and 8) and the effects of acoustic excitation on jets (Ref. 9). Morris et al.[10] have argued that it is the linear contributions to the vortex forces in a turbulent flow that dominate the interaction between the fluctuating and mean flows. The present model for turbulent mixing in compressible axisymmetric shear layers is an extension of this last work. Thus, some details of this model are given here.

Morris et al.[10] assumed that the characteristic shape of the mean velocity and density profiles were known. The development of the mean flow could then be described in terms of local scales: the width of the shear layer and the location of the half-velocity point. The integral mean momentum and mechanical energy equations then yielded ordinary differential equations for the streamwise evolution of these scales. The large-scale structures were modeled as a superposition of instability waves. The local characteristics of these waves were determined from the solution of the linear, inviscid, stability, or Rayleigh equation. Two models were used to simulate the development of the shear layer. In the first, which modeled the average evolution of the shear layer, the large-scale turbulence spectrum was represented by a random superposition of instability waves with a broad range of frequencies and spanwise wave numbers. In the second, the subharmonic evolution model proposed by Ho and Huang[11] was used to represent the passage of a single train of large-scale structures. In this case, the large-scale structures were described by the sum of a set of discrete frequency waves. The frequencies corresponded to the initial shedding frequency and its subharmonics. The process of energy transfer from the large to small scales was described by two very crude models. In the first, the energy associated with a given wave was removed at the streamwise location where it became neutrally stable according to linear theory. In the second, the wave was permitted to decay smoothly with the use of a simple eddy-viscosity model. There was little difference between the predictions for the mean flow development based on these two models. Thus, it was shown that the details of the energy transfer process are relatively unimportant to the development of the flow at the large scale. Since the instability waves are determined locally from a linear analysis, this does not provide a prediction of their amplitude. This was obtained from the energy integral equation for the large-scale fluctuations. Thus, the development of the large-scale structures was determined from a weakly nonlinear analysis. Predictions of the rate of growth of the shear layer as a function of freestream Mach numbers and density and velocity ratios showed excellent agreement with experiment. Predictions of the time-dependent flow at the large scale based on the subharmonic evolution model showed qualitative agreement with experimental observations. It is important to note that these models contained no empirical constants. Thus, some confidence can be felt that the important physical processes that control the mixing in free shear flows were captured.

A number of recent studies, such as those by Zhuang et al.,[12] Sandham and Reynolds,[13] and Ragab and Wu,[14] have shown how the decrease in the rate of spread of a shear layer with increase in the convective Mach number may be correlated with the maximum amplification rate predicted by linear instability theory. The present analysis for the axisymmetric shear layer and that of Morris et al.[10] for the plane shear layer

Received Sept. 12, 1990; revision received Sept. 20, 1991; accepted for publication Sept. 21, 1991.

*Research Associate, Department of Aerospace Engineering. Member AIAA.

†Boeing Professor, Department of Aerospace Engineering. Associate Fellow AIAA.

show why this correlation is to be expected. In addition, these latter models make predictions of the absolute rate of growth of the shear layers not their rates of growth relative to their incompressible values.

In the next section, the model equations are derived and the assumptions of the model are presented and discussed. Section III describes the calculation procedure and the results. Predictions are made for the effect of freestream Mach number and velocity ratio on the growth of the axisymmetric shear layer. The effects of the choice of initial shear layer thickness and the initial amplitudes of the instability waves are shown. The effect of the choice of shape for the mean velocity profile is also described. Comparisons between the predictions and experimental measurements in both plane and axisymmetric shear layers are presented. Section IV provides a discussion of the predictions and a description of ongoing extensions to the models.

II. Model Equations

In this section, a brief derivation of the model equations for the turbulent mixing of a supersonic jet in a coflowing stream are presented. The equations are written in cylindrical polar coordinates (r, θ, z) with the origin at the center of the jet exit and the z axis aligned with the jet centerline. The jet is assumed to be operating on-design and the mean static pressure is taken to be constant throughout the flow. It is also assumed that the local Mach number is sufficiently low for the density-velocity correlations to be neglected with respect to the velocity-velocity correlations in the mean equations. This follows the arguments of Morkovin[15] and Bradshaw.[16] In the latter study, which considered free shear flows, it was argued that a local Mach number of 1.5 was the upper limit for the neglect of these correlations. Recently, Morkovin[17] has emphasized the differences between Mach number effects in boundary layers and free shear layers. In the latter case, the limit on the upstream region of influence may have a profound influence on the turbulent structure. For example, coherent vortex roll-up might be inhibited. It is these kinds of dynamic effects that may be modeled in the present approach that may not be described by traditional Reynolds stress closure schemes.

The averaged inviscid, compressible equations of continuity, momentum, and mechanical energy are simplified using an order of magnitude analysis for thin shear layers. The resulting equations may be written as,

$$\frac{1}{r}\frac{\partial(\bar{\rho}\bar{u}r)}{\partial r} + \frac{\partial(\bar{\rho}\bar{w})}{\partial z} = 0 \tag{1}$$

$$\bar{\rho}\bar{u}\frac{\partial \bar{w}}{\partial r} + \bar{\rho}\bar{w}\frac{\partial \bar{w}}{\partial z} = -\frac{1}{r}\frac{\partial(\overline{\bar{\rho}u'w'}r)}{\partial r} \tag{2}$$

$$\bar{\rho}\bar{u}\frac{\partial \bar{w}^2}{\partial r} + \bar{\rho}\bar{w}\frac{\partial \bar{w}^2}{\partial z} = -\frac{2\bar{w}}{r}\frac{\partial(\overline{\bar{\rho}u'w'}r)}{\partial r} \tag{3}$$

The overbar denotes a long-time averaged quantity and the prime denotes a fluctuation about this mean; (u, v, w) are the velocity components in the (r, θ, z) directions, respectively. All of the variables have been nondimensionalized with respect to the jet exit velocity w_j, the jet exit density ρ_j, and the jet exit radius r_j.

It is assumed that the mean velocity in the axial direction and the mean density may be written in a self-similar form such that,

$$\bar{w} = R + (1 - R)f(\eta) \tag{4a}$$

$$\bar{\rho} = g(\eta; R, s) \tag{4b}$$

where

$$\eta = \frac{r - h(z)}{b(z)} \tag{4c}$$

Here, $R = w_2/w_j$ is the velocity ratio and $s = \rho_2/\rho_j$ is the density ratio, where w_2 and ρ_2 are the axial velocity and density in the coflowing stream, respectively. Also, $h(z)$ and $b(z)$ are the potential core radius and the half-velocity thickness of the jet, respectively.

The assumed forms of mean velocity and density profiles may be substituted into the governing equations (1-3), and the spatial derivatives may be rewritten in terms of the similarity coordinate η. The continuity equation is then integrated to yield an expression for $\bar{\rho}\bar{u}$. This is substituted into the momentum and energy equations. These equations are then integrated with respect to η from the jet axis to infinity. Integration by parts gives the following equations,

$$(1 - R)h\frac{dh}{dz} + 2b\frac{db}{dz}\beta_2 + \frac{d(hb)}{dz}\beta_1 = 0 \tag{5}$$

$$h\frac{dh}{dz}(1 - R^2) + 2b\frac{db}{dz}\beta_4 + \frac{d(hb)}{dz}\beta_3 = 2\int_0^\infty \overline{gu'w'}(b\eta + h)\frac{df}{d\eta}d\eta \tag{6}$$

where β_1, β_2, β_3, and β_4 are integrals involving the mean velocity and density shape functions $f(\eta)$ and $g(\eta)$. They are defined in the Appendix. If Eq. (5) is integrated with respect to z and the initial conditions are imposed that $h(0) = 1$ and $b(0) = 0$, an algebraic relationship may be obtained between h and b. This may be written as,

$$(1 - R)(h^2 - 1) + 2hb\beta_1 + 2b^2\beta_2 = 0 \tag{7}$$

This may be used to eliminate dh/dz from Eq. (6) and provide a single ordinary differential equation for db/dz. The integral on the right-hand side of Eq. (6) represents the rate of production of turbulent energy. This term has to be modeled in order to predict the development of the mean flow.

As discussed in the Introduction, the large-scale structures are assumed to dominate the turbulent mixing process in free shear flows. In addition, these structures may be described by a superposition of instability waves. The form of these wave-like fluctuations is taken to be

$$\phi'(r, \theta, z, t) = A(z)\Re\{\hat{\phi}(r)\exp[i(\alpha z + n\theta - \omega t)]\} \tag{8}$$

where ϕ' is any large-scale fluctuation, $A(z)$ the amplitude of the instability wave, ω the (real) radian frequency, α the (complex) axial wave number, n the azimuthal mode number, and $\Re$ denotes the real part of a function. Fluctuations of this form are introduced into the linearized Euler equations. A locally parallel approximation is made for the mean velocity and density. The fluctuating pressure is then found to satisfy the compressible Rayleigh equation,

$$\frac{d^2\hat{p}}{dr^2} + \left[\frac{1}{r} - \frac{1}{\bar{\rho}}\frac{d\bar{\rho}}{dr} - \frac{2\alpha}{(\alpha\bar{w} - \omega)}\frac{d\bar{w}}{dr}\right]\frac{d\hat{p}}{dr} + \left[\bar{\rho}M_j^2(\alpha\bar{w} - \omega)^2 - \frac{n^2}{r^2} - \alpha^2\right]\hat{p} = 0 \tag{9}$$

In regions of constant mean flow properties, that is, in the potential core or in the fluid surrounding the jet, the solutions to Eq. (9) are of the form,

$$\hat{p} = \begin{cases} J_n(i\lambda_j r), & \text{for } r \le h \\ H_n^{(1)}(i\lambda_o r), & \text{for } r \to \infty \end{cases} \tag{10}$$

where

$$\lambda_j = \sqrt{\alpha^2 - M_j^2(\alpha - \omega)^2} \tag{11}$$

$$\lambda_o = \sqrt{\alpha^2 - sM_j^2(\alpha R - \omega)^2} \tag{12}$$

The branch cut for the square root of λ_o is chosen to insure decaying solutions or outgoing waves as $r \to \infty$. J_n is the Bessel function of the first kind and order n, and $H_n^{(1)}$ is the Hankel function of the first kind and order n.

An equation for the axial development of the instability wave amplitude $A(z)$ may be obtained from the kinetic energy equation for the large-scale motions. This may be obtained by subtracting the mean energy equation from the instantaneous energy equation. In Cartesian tensors, the kinetic energy equation for the large-scale structures may be written as,

$$\bar{\rho}\bar{u}_j \frac{\partial \bar{k}}{\partial x_j} = -\overline{\rho u_i' u_j'} \frac{\partial \bar{u}_i}{\partial x_j} - \frac{\partial \overline{u_i' p'}}{\partial x_i} + \overline{p' \frac{\partial u_i'}{\partial x_i}} \tag{13}$$

where $\bar{k} = \overline{u_i' u_i'}/2$. The first term on the right-hand side represents the production of large-scale kinetic energy and the last two terms represent the pressure work. At this stage, it would be possible to integrate the equation with respect to r to obtain the energy integral equation. However, in the present case, as will be seen later, it is convenient to rearrange the equation as follows. The last term in Eq. (13) may also be obtained by multiplication of the energy equation for the large-scale motions by p'. The time average of the resulting equation may be written as,

$$\overline{p' \frac{\partial u_i'}{\partial x_i}} = -\frac{M_j^2}{2} \frac{\partial}{\partial x_j} (\bar{u}_j \overline{p'^2}) - \frac{(2\gamma - 1)}{2} M_j^2 \overline{p'^2} \frac{\partial \bar{u}_j}{\partial x_j} \tag{14}$$

Now, for a parallel mean flow, or a mean flow in which the mean density or temperature does not vary significantly, the last term in Eq. (14) may be neglected. Then, with Eq. (14), the integration of Eq. (13) with respect to r from 0 to ∞ yields,

$$\frac{\mathrm{d}}{\mathrm{d}x} \int_0^\infty \left[\bar{\rho}\bar{w}\bar{k} + \overline{w'p'} + \frac{M_j^2}{2} \bar{w} \overline{p'^2} \right] r \, \mathrm{d}r = -\int_0^\infty \bar{\rho} \overline{u'w'} \frac{\partial \bar{w}}{\partial r} r \, \mathrm{d}r \tag{15}$$

It should be noted that the terms on the left-hand side of Eq. (15) represent both the integrated kinetic energy flux and the pressure work. Though, in this form, there is no distinction between transport and source terms, it is a convenient form for the present models.

Substitution of fluctuations of the form of Eq. (8) into Eq. (15) yields,

$$\frac{\mathrm{d}}{\mathrm{d}z} [b^2 A^2 I_1] = -A^2 (b k_2 + h k_1) \tag{16}$$

where k_1 and k_2 are defined in the Appendix, and I_1 is given by

$$I_1 = \int_0^\infty \left[\frac{1}{4} \bar{\rho} \bar{w} (|\hat{u}|^2 + |\hat{v}|^2 + |\hat{w}|^2) + \frac{\bar{w} M_j^2}{4\bar{\rho}} |\hat{p}|^2 + \frac{1}{2} \Re \{ \hat{p} \hat{w}^* \} \right] r \, \mathrm{d}r \tag{17}$$

Since the local descriptions of the fluctuations are obtained from a linear equation, they may be normalized in any convenient manner. In the present case, they are normalized such that,

$$I_1 = 1 \tag{18}$$

It should be noted that Eq. (16) is valid for either a parallel or a diverging mean flow. If the flow were actually parallel, then the rate of change of amplitude with downstream distance would be related to the imaginary part of the eigenvalue. That is,

$$\frac{1}{A^2} \frac{\mathrm{d}A^2}{\mathrm{d}z} = -2\alpha_i \tag{19}$$

Since, in the present calculations, the large-scale structures are approximated locally by a parallel flow approximation, it is clear that the integrals on the right-hand side of Eq. (16) are given by

$$b(z)k_2(z) + h(z)k_1(z) = 2b^2(z)\alpha_i(z) \tag{20}$$

Thus, it is not necessary to calculate the eigenfunctions and perform the integrations to obtain k_1 and k_2 in order to calculate the development of the mean flow. Substitution of Eq. (20) into Eq. (16) then yields,

$$\frac{\mathrm{d}A^2}{\mathrm{d}z} = -2 \left\{ \alpha_i + \frac{1}{b} \frac{\mathrm{d}b}{\mathrm{d}z} \right\} A^2 \tag{21}$$

The preceding analysis provides a simple correction for the effects of flow divergence on the growth of the instability waves. However, it should be noted that the prediction of the effects of flow divergence based on a multiple scales technique also uses the parallel flow approximation eigenfunctions to determine the first-order correction. The present method of correction is equivalent to the energy method perturbation technique.

It should be noted that the integrals on the right-hand sides of Eqs. (6) and (15) are identical except for a change of sign. Thus, the integral on the right-hand side of Eq. (6) may also be related to the amplitude of the instability waves and the local eigenvalues. Equations (5), (6), and (21) may now be used to describe the axial development of the mean flow and the instability waves. As described earlier, two models are used here. In the first, the broadband model, which simulates the average development of the mean flow, the large-scale structures are represented by a broad spectrum of frequencies and azimuthal mode numbers. The evolution of each spectral component is assumed to be given by Eq. (21), and the development of the mean flow is controlled by the total transfer of energy to the large-scale motions. If $h(z)$ is eliminated between Eqs. (5) and (6), the following set of equations for the axial evolution of the mean flow and the instability wave amplitudes may be obtained,

$$\frac{\mathrm{d}}{\mathrm{d}z} A^2(z;\omega,n) = -2 \left\{ \alpha_i(\omega,n) + \frac{1}{b} \frac{\mathrm{d}b}{\mathrm{d}z} \right\} A^2(z;\omega,n) \tag{22}$$

$$\frac{\mathrm{d}b}{\mathrm{d}z} = \frac{4b^2}{k_3} \sum_{n=-N}^{N} \int_0^\infty \alpha_i(\omega,n) A^2(z;\omega,n) \, \mathrm{d}\omega \tag{23}$$

In this case, the amplitude $A(z)$ represents a spectral density component of the axial flux of large-scale energy. The expression for k_3 is given in the Appendix. In the case of the subharmonic model, the evolution equations may be written as,

$$\frac{\mathrm{d}}{\mathrm{d}z} A_j^2 = -2 \left\{ [\alpha_i]_j + \frac{1}{b} \frac{\mathrm{d}b}{\mathrm{d}z} \right\} A_j^2 \tag{24}$$

$$\frac{\mathrm{d}b}{\mathrm{d}z} = \frac{4b^2}{k_3} \sum_{n=-N}^{N} \sum_{j=1}^{M} [\alpha_i]_j A_j^2 \tag{25}$$

where the subscript j refers to the jth instability wave. In both models, it has been assumed that there is sufficient jitter in the phase between the different spectral components so that strong intercomponent coupling does not occur. M represents the number of subharmonic components in the model, and N represents the number of azimuthal modes.

In the case of a two-dimensional shear layer, the equivalent equations in the subharmonic model case are given in Ref. 10 as,

$$\frac{\mathrm{d}}{\mathrm{d}x} B_j^2 = -2 \left\{ 2[\alpha_i]_j + \frac{1}{\delta} \frac{\mathrm{d}\delta}{\mathrm{d}x} \right\} B_j^2 \tag{26}$$

$$\frac{\mathrm{d}\delta}{\mathrm{d}x} = -\frac{4\delta}{k_4} \sum_{j=1}^{N} [\alpha_i]_j B_j^2 \tag{27}$$

where an expression for k_4 is given in the Appendix, and x is the downstream distance. In the two-dimensional case, δB_j^2 represents the energy flux per unit width of the shear layer for the jth instability wave. In the axisymmetric case, $2\pi b^2 A_j^2$ represents the total energy flux of the jth instability wave at a given axial location. In the two-dimensional model, the local similarity coordinate takes the form,

$$\eta = [y - y_0(x)/\delta(x)] \tag{28}$$

where $y_0(x)$ is the location of the half-velocity point, and $\delta(x)$ is a measure of the width of the shear layer.

In the next section, the evaluation of the coefficients in these equations for both the axisymmetric and plane shear layers is described, and predictions for the axial evolution of the mean flow and the instability wave amplitudes are given.

III. Calculation Procedure and Results

Before proceeding with the calculation of the axial development of the axisymmetric shear layer, it is necessary to specify the shape of the mean velocity and density profiles defined in Eq. (4). The shape function for the mean velocity is taken to be of the form,

$$f(\eta) = \begin{cases} 1, & \text{if } \eta < 0 \\ \exp[-\ell n(2)\eta^2], & \text{if } \eta \geq 0 \end{cases} \tag{29}$$

The mean density is related to the mean velocity by a Crocco-Busemann relationship. This assumes a Prandtl number of unity and constant mean static pressure. Then the mean density is given by

$$\bar{\rho} = g(\eta;R,s) = \left[-\kappa\bar{w}^2 + \left\{\left(\frac{s-1}{s}\right) + \kappa(1-R^2)\right\}\frac{1}{(1-R)}\bar{w} + \frac{1}{2}\left\{\left(\frac{s+1}{s}\right) + \kappa(1+R^2) - \frac{(1+R)}{(1-R)}\left[\left(\frac{s-1}{s}\right) + \kappa(1-R^2)\right]\right\}\right]^{-1} \tag{30}$$

where $\kappa = (\gamma - 1)M_j^2/2$. In the two-dimensional case, the mean velocity profile is represented by

$$f(\eta) = \tfrac{1}{2}(1 + \tanh \eta) \tag{31}$$

unless noted otherwise. As a common basis for comparison of the spreading rates of the two-dimensional and axisymmetric shear layers, the vorticity thickness δ_ω is used. This is defined as the velocity difference divided by the magnitude of the maximum velocity gradient. For the chosen form of velocity profiles, it is readily shown that,

$$\delta_\omega = 1.400b = 2\delta \tag{32}$$

For a given set of operating conditions, M_j, R, and s, the Rayleigh equation (9) may be solved for various values of local thickness $b(z)$ for each azimuthal mode number and frequency. The relationship between $b(z)$ and the potential core radius $h(z)$ is given by Eq. (7). A fifth-order Runge-Kutta-Felberg algorithm is used to integrate Eq. (9) from the edge of the potential core ($\eta = 0$) outward and the outer edge of the jet shear layer ($\eta \approx 3.2$) inward. The forms of the initial conditions are given by Eq. (10). At the half-velocity point, $\eta = 1$, the numerical solutions are matched to find their unknown coefficients. For a nontrivial solution, the determinant of the matrix equation for the coefficients must be zero. The value of the wave number α is varied iteratively until this condition is met. The eigenvalues for decaying waves, $\alpha_i > 0$, are found by integration along a contour in the complex r plane that avoids the critical point of the Rayleigh equation and its branch cut. Further details are given in Tam and Morris.[18]

For the subharmonic evolution model, the instability wave frequencies are chosen to be the initially most unstable frequency for each azimuthal mode and its subharmonics. The initially most unstable frequency corresponds closely to the observed shedding frequency. The azimuthal modes included in the present calculations are the axisymmetric, $n = 0$, mode, and the helical, $n = \pm 1$, mode. These are observed to dominate the large-scale motions in jets. In the present case, a total of 75 frequencies are chosen for each azimuthal mode number. Once again, only the $n = 0$ and ± 1 modes are included. These frequencies are taken to be less than the neutrally stable frequency at the jet exit. It may be argued that higher-frequency components would decay rapidly and not contribute significantly to the large-scale spectrum farther downstream In both models, the initial amplitudes of each instability wave or spectral component are taken to be equal.

From the stored values of $[\alpha_i]_j$ or $\alpha_i(\omega,n)$ as a function of $b(z)$, it is possible to solve Eqs. (22) and (23) or Eqs. (24) and (25) for given initial values of $b(0)$ and $A_j(0)$ or $A(0;\omega,n)$ by marching in the axial direction. The results of a typical calculation are shown in Fig. 1. The operating conditions in this case are $M_j = 0.25$, $R = 0.25$, and $s = 1$. The model used in this case is the subharmonic evolution model. The axial evolution of both the $n = 0$ and 1 instability waves are shown. The fundamental frequency wave and two subharmonics are used in this calculation. In this case of relatively low Mach number, the axial evolution of the axisymmetric and helical models is similar, particularly in the initial shear layer. Farther downstream, the helical mode achieves a greater amplitude. Beyond the end of the potential core only the helical mode is unstable. However, the present calculations are confined to the axisymmetric shear layer surrounding the potential core. At higher Mach numbers, the stability characteristics of the axisymmetric and helical waves are not similar, and in many cases, the helical mode dominates. Since only two subharmonics have been included in this calculation, the axial development of the mean flow has only been predicted up to the point where the next subharmonic might be expected to contribute to the energy exchange with the mean flow. The growth of the shear layer thickness is seen to proceed in steps with a region of relatively rapid growth followed by a plateau. This is characteristic of the growth of an excited shear layer. Ho and Huang[11] observed that this plateau occurred following the pairing of two vortices in the shear layer. It also corresponded to a saturation in amplitude of the subharmonic frequency. This is also seen in the present calculations where the first subharmonic peaks at $x/r_j \approx 3$, and this is followed by a region of relatively slow axial growth.

The rate of growth of the shear layer may be obtained by fitting a straight line to the shear-layer thickness calculations, excluding the initial development region. This gives $db/dz \approx 0.063$ or $d\delta_\omega/dz \approx 0.088$. This is consistent with the calculations for the effects of velocity ratio to be shown later. Different initial jet widths and instability wave amplitudes have been considered. In the calculation shown in Fig. 1, $b(0) = 0.05$ and $A_j(0) = 0.01$. For the different initial widths and amplitudes, no appreciable difference was found in the predicted rate of jet spread. However, some differences were observed in the initial development region, and the virtual origin of mixing changed.

Figure 2 shows the predicted axial variation of the half-velocity thickness of an axisymmetric shear layer. The predictions are compared with the experimental measurements of Lepicovsky et al.[5] Predictions are shown for both the broadband model and the subharmonic evolution model. The agreement between the predictions and the measurements in both cases is very good. However, it should be noted that the present calculations are only valid in the annular mixing region surrounding the potential core. The observed length of the potential core was between 10 and 12 diameters. In the present case, Eq. (7) indicates that the end of the potential core, where $h = 0$, occurs at $b/r_j = 1.28$. Thus, it is clear that

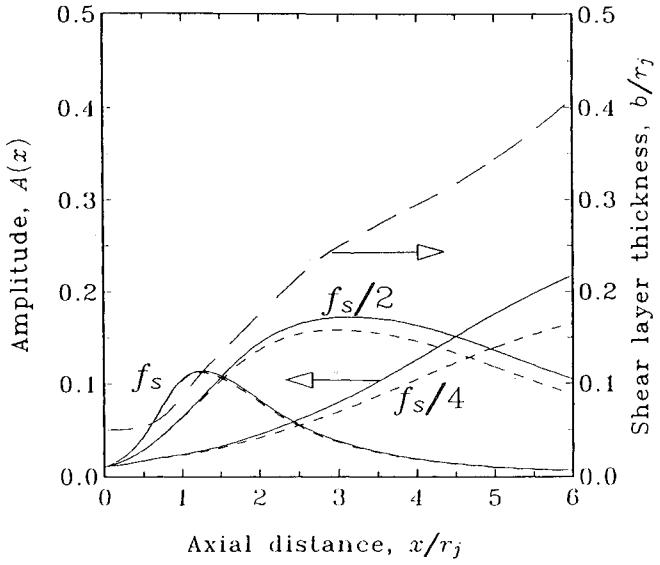

Fig. 1 Variation of shear-layer thickness and amplitude with axial distance: $M_j = 0.25$; $R = 0.25$; $s = 1.0$; ——— shear layer thickness; —— axisymmetric mode; - - - - - helical mode.

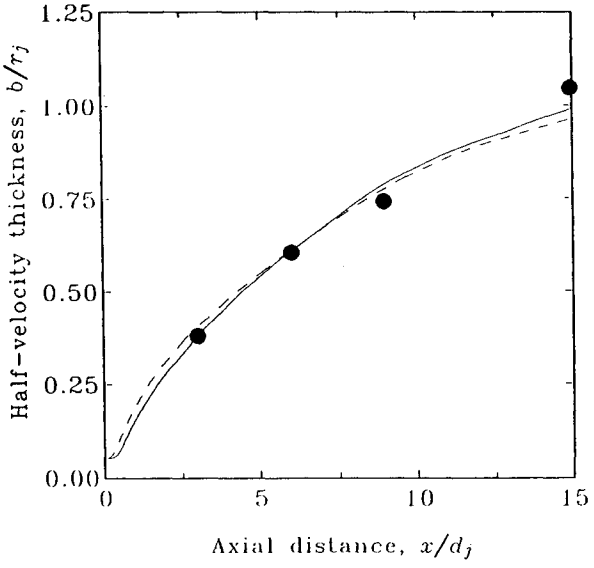

Fig. 2 Variation of half-velocity thickness with downstream distance: —— subharmonic evolution model; - - - - - broadband model; ● Lepicovsky et al.[5]; $M_j = 1.4$; $R = 0.0$; $s = 0.72$.

the agreement between the predictions and the measurements for $x/d_j > 10$ is probably fortuitous. There are two reasons for this. It is to be expected that, near the end of the potential core, the jet velocity profile undergoes a transition between its annular form and the fully developed jet form. Thus, the mean velocity profile should be a function of both the width of the jet shear layer and the centerline velocity. Also, the number of amplifying instability waves of low frequency, included in the present calculations, decreases with axial distance. This tends to decrease the energy transfer from the mean flow to the large-scale structures and results in a decrease in the rate of spread of the jet. Both of these deficiencies could be corrected by a suitable choice of mean velocity profile in the transition region and the inclusion of additional low-frequency components in the broadband model or lower subharmonics in the subharmonic evolution model. However, the agreement between the measurements and predictions in the annular shear layer provides a good validation of the present model.

Figure 3 shows the effect of the choice of initial amplitude on the evolution of the axisymmetric shear layer. The predictions are again compared with the measurements of Lepicovsky et al.[5] The broadband model is used in these predictions. As the initial amplitude of the spectrum increases, the axial location at which the shear layer begins to spread moves closer to the jet exit. However, once the initial development region is passed, the spreading rate of the shear layer is essentially independent of the initial spectrum level.

Observations in both shear layers and jets have shown that, as the Mach number increases, the rate of growth of the shear layer decreases. Bogdanoff[19] and Papamoschou and Roshko[6] have proposed that the convective Mach number is the proper parameter to correlate the effects of compressibility on turbulent mixing in free shear flows. The convective Mach number is defined as the relative velocity between the large-scale structures and the freestream divided by the freestream speed of sound. If it is assumed that in a frame of reference traveling with the large structures there is a stagnation point between the structure and the flow decelerates isentropically to the stagnation point, an expression may be obtained for the convective Mach numbers in terms of the operating conditions alone. It should be noted that experimental observations indicate that this assumption is incorrect and the actual convective Mach numbers of the structures differ from this isentropic value (see Ref. 20). In the present calculations, no such assumptions are necessary as the convection velocity of the large structures is taken to be the average phase velocity of the instability wave that is dominant in any region. The definitions of the convective Mach numbers are

$$M_{cj} = (1 - c)M_j, \qquad M_{co} = \frac{(c - R)M_j\sqrt{s}}{\sqrt{\gamma_o/\gamma_j}} \tag{33}$$

where c is the average phase velocity of the locally dominant instability wave given by $c = \omega/\alpha_r$, and γ_j and γ_o are the specific heat ratios of the jet and the coflowing stream, respectively. M_{cj} is the convective Mach number with respect to the jet, and M_{co} is the convective Mach number with respect to the coflowing stream. Unless otherwise noted, $\gamma_j = \gamma_o$ in the subsequent calculations. For convenience, the results in this section are presented with respect to a geometric average of the two Mach numbers following Messersmith et al.[21] Thus, the convective Mach number is taken to be given by

$$M_c = \sqrt{M_{cj}M_{co}} \tag{34}$$

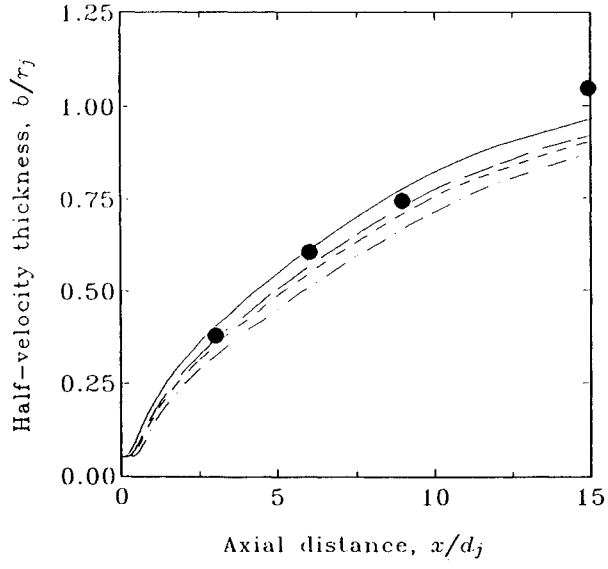

Fig. 3 Effect of initial amplitude on jet spread rate: —— $A(0) = 0.038$; ——— 0.022; - - - - - 0.017; — - — 0.010; ● Lepicovsky et al.[5]; $M_j = 1.4$, $R = 0.0$, $s = 0.72$.

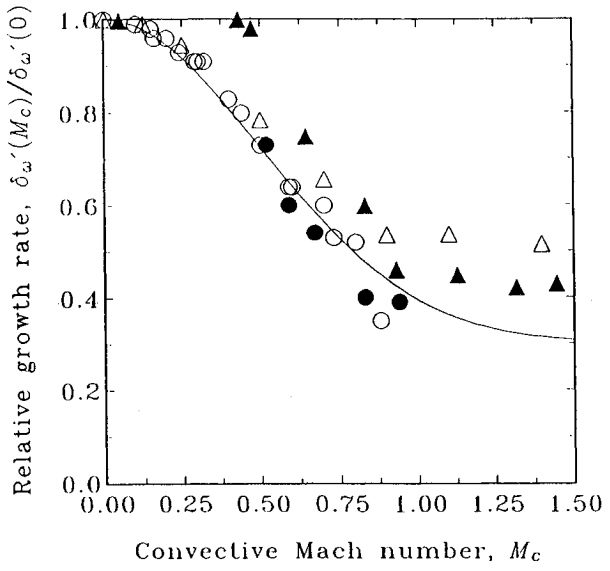

Fig. 4 Variation of vorticity thickness growth rate with convective Mach number. Predictions for various values of R and s: ○ plane; △ axisymmetric; ● Chinzei et al.[29]; ▲ Bogdanoff[19]; —— curve fit, Messersmith et al.[21]

Figure 4 shows the predicted vorticity thickness growth rates, relative to their zero convective Mach number values, as a function of convective Mach number. Also shown are calculations for the two-dimensional shear layer from Ref. 10 and experimental observations from several investigations. The agreement between the predictions and the experiments is very good. As the convective Mach number increases, the relative growth rate decreases until the convective Mach number approaches unity. Beyond this value, both the predictions and the experiments indicate a near independence of the growth rate on the convective Mach number. However, the predictions for the two-dimensional shear layer continue to fall. This is because the calculations of Ref. 10 included only two-dimensional instability waves. However, it is known that, as the convective Mach number increases, the most unstable instability waves are three dimensional. Thus, it is not surprising that the two-dimensional calculations underpredict the growth rate of the shear layer. It should be noted that more recent predictions for the two-dimensional shear layer by Giridharan and Morris,[22] which include three-dimensional instability waves, also show a leveling off of the relative growth rate for supersonic convective Mach numbers. For example, they predict that $\delta'_\omega(M_c)/\delta'_\omega(0) = 0.4$ for $M_c = 1.8$. The axisymmetric shear-layer calculations shown here include three-dimensional instability waves: the helical instabilities. Thus, the model should be expected to provide valid predictions at supersonic convective Mach numbers.

It should be noted that other authors, including Sandham and Reynolds[13] and Ragab and Wu,[14] have noted the similarity between the observed relative decrease in the shear-layer growth rate with convective Mach number and the change in the ratio of the maximum amplification factor $[\alpha_i]_{\max}$ at a given convective Mach number and its incompressible value. The present calculations make predictions of the actual growth rate of the shear layer rather than the maximum instability wave growth rate. Thus, the present comparisons with experiments are comparing like quantities. However, it is clear from either Eq. (23) or (25) that there is a close relationship between the rate of growth of the shear layer and the amplification rate of the instability waves. Also, as k_3 varies nearly linearly with shear-layer thickness b and $[\alpha_i]_j b$ is nearly independent of b downstream of the initial development region, the rate of growth of the shear layer is nearly linear and proportional to the local amplification rate of the dominant instability.

As noted earlier, the present calculations make predictions of the absolute rate of growth of the axisymmetric shear layer. In the incompressible limit, the rate of growth of both a two-dimensional and an axisymmetric shear layer are functions of the velocity and density ratio. The present calculations indicate that the effect of velocity ratio on the growth of the shear layer is different in the two-dimensional and the axisymmetric case. Figure 5 shows a comparison between the two-dimensional (from Ref. 10) and the present predictions of the variation in vorticity thickness growth rate with velocity ratio. Both sets of predictions are compared with experiments and are shown as varying with the velocity ratio parameter λ defined by

$$\lambda = \frac{(1-R)}{(1+R)} \tag{35}$$

It may be seen that there are differences between the actual growth rates in the two cases. There appear to be very few experimental studies of the initial development of an axisym-

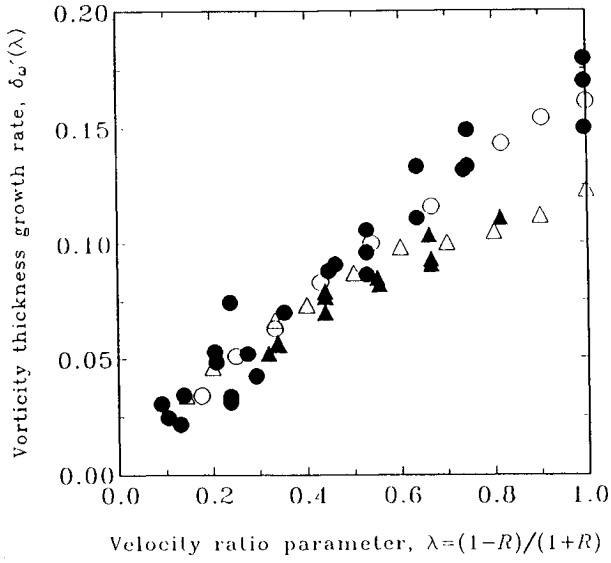

Fig. 5 Variation of vorticity thickness growth rate with velocity ratio parameter: ○ plane; △ axisymmetric; ● Brown and Roshko[1]; ▲ Morris.[23]

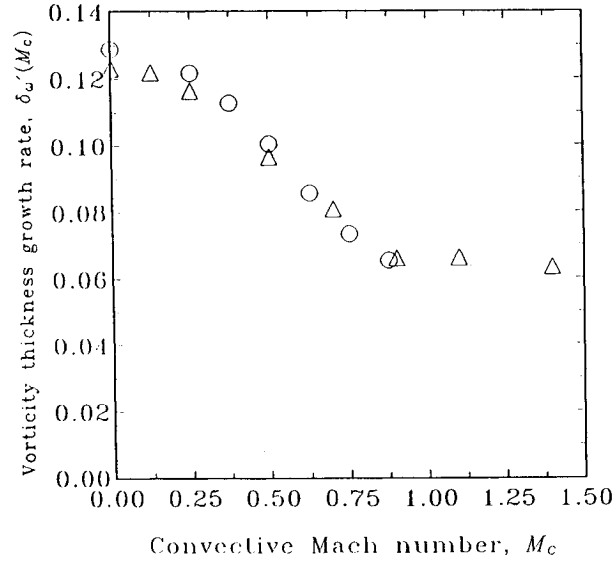

Fig. 6 Variation of vorticity thickness growth rate with convective Mach number. Both calculations use the half-Gaussian velocity profile: $R = 0$; $s = 1$; ○ plane; △ axisymmetric.

metric jet in a coflowing stream. However, the measurements by Morris[23] for a circular jet with $M_j = 0.47$ are shown. Both the experiments and predictions indicate a lower value for the vorticity thickness growth rate for the axisymmetric shear layer at all velocity ratios. It should be noted that the agreement between the predictions and experiment in both cases is extremely good. Since the predictions are based on a model for the turbulent mixing process that contains no empirical constants, these results give some confidence that the present models provide a correct description of the important physical phenomena present in the mixing process.

It is possible to explain the predicted and measured differences between the two-dimensional and axisymmetric cases if the choice of mean velocity profile shape is examined. Figure 6 shows a comparison between the predicted two-dimensional and axisymmetric shear-layer growth rates as a function of convective Mach number. However, in these calculations, the velocity profile in the two-dimensional case is also taken to have a half-Gaussian form as defined in Eq. (29). There is a very good agreement between the predicted spread rates of the axisymmetric and two-dimensional shear layers. This is not unexpected as, in the initial mixing region where the shear-layer thickness is very small, the axisymmetric shear layer should behave like a plane shear layer. It should be noted that in these calculations care had to be taken that the initial energy levels of the large-scale structures were the same in order to insure complete agreement between the plane and axisymmetric cases. This meant that the initial values of A_j^2 in Eq. (24) and B_j^2 in Eq. (26) were not the same. This is because, as noted earlier in Sec. II, they represent different quantities. Thus, the growth rates of the shear layers depend on the detailed shape of the mean velocity profile. Experimental observations show that the choice of mean velocity profile shapes given by Eq. (29) for the axisymmetric shear layer and Eq. (31) for the plane shear layer are in good agreement with experiment. It is clear that, in general, it would be desirable to calculate the mean velocity profile. The turbulence model would then be truly predictive in nature. This is discussed in Sec. IV.

Finally, Fig. 7 shows the predicted variation of the vorticity thickness growth rate with convective Mach number for three different velocity ratios. The rate of growth of the shear layer decreases with increasing convective Mach number and increasing velocity ratio. If the predictions were nondimensionalized with respect to their incompressible values, they would collapse onto a single curve, as shown in Fig. 4. However, the method of presentation in Fig. 7, showing the absolute value of the growth rate, emphasizes that the growth rate is a strong function of velocity ratio. This can be as important a factor as the convective Mach number in setting the actual growth rate. For example, a shear layer with $M_c = 0$ and $R = 0.5$ has the same growth rate as a shear layer with $M_c = 1.4$ and $R = 0$. There is a qualitative agreement between these predictions and the experimental observations of Gutmark et al.[24] A direct comparison with the measurements is not possible since the spreading rate measurements were based on total pressure. This includes both the velocity and density gradients in the radial direction. The predicted vorticity thickness is based solely on the velocity gradient.

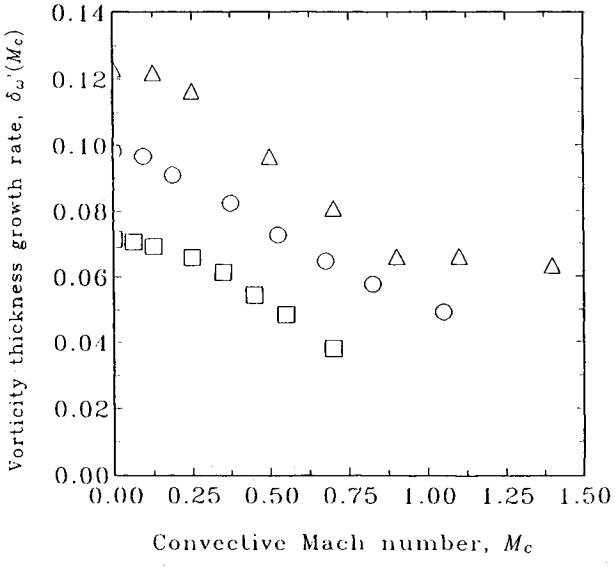

Fig. 7 Variation of vorticity thickness growth rate with convective Mach number: △ $R = 0.0$; ○ $R = 0.25$; □ $R = 0.5$.

IV. Summary and Discussion

From the predictions of this paper, it is clear that the development of free shear layers is related closely to the stability characteristics of the mean flow. The features of the large-scale structures and their role in the mixing process are predicted well by an inviscid analysis. This analysis captures the decrease in the production of turbulent energy as the convective Mach number increases. The model takes no account of the details of the energy transfer process from large to small scales or its eventual viscous dissipation. It should be emphasized that the present model captures the important features of the mixing process in free shear flows. In particular, it predicts the reduction in mixing that occurs with the increase in convective Mach number. The present model should be contrasted with other models for compressible turbulent flows, such as Sarkar et al.[25] and Sarkar and Balakrishnan.[26] In these conventional Reynolds stress closure models, a simple algebraic model is used to describe the compressible dissipation. This is the component of the total viscous dissipation rate associated with the fluctuating dilatation. This model is based on an asymptotic theory for low-turbulent Mach numbers and has been validated against full numerical simulations of isotropic turbulence (see Ref. 27). However, such models do not capture the dynamics of the turbulent mixing process that is lost in the averaging procedure. For free shear flows that are strongly dynamically unstable, it is likely that the present model captures the important physics. For other turbulent flows that do not possess such a strong instability, it is likely that other compressibility effects, such as those proposed by Sarkar et al.,[25] may be dominant.

The present calculations indicate that the initial rate of spread of the axisymmetric shear layer is less than that of the plane shear layer. This is related to the different characteristic mean velocity profiles in the two cases. It might be expected that this difference might persist farther downstream as the axisymmetric shear layer and the developed jet are less dynamically unstable than the two-dimensional shear layer. However, it is not clear that the contribution to the total Reynolds stress from the small scale motions might not be significant in the jet development farther downstream. As noted earlier, the extension of the present model to this region is possible if a suitable form for the mean velocity profile is chosen and sufficiently low frequencies are included in the model for the large-scale motions. The validity of the model in the developed jet could then be tested. However, in the initial region of the jet, both the subharmonic evolution model and the broadband model are in good agreement with experiments. It should be emphasized that these models for the development of the axisymmetric shear layer and the turbulent mixing at the large scale contain no model constants.

Though the present calculations provide good agreement with experiment and provide an explanation of the changes in the turbulent mixing process in compressible shear layers, they are not a full turbulence closure scheme. Some assumptions must be made regarding the characteristic shape of the mean velocity and density field. Recent calculations by Liou and Morris[28] have shown that the models may be implemented in differential form. In that case, the mean velocity profile is predicted simultaneously with the large-scale structures.

Appendix: Definitions

The integrals and coefficients required for the axisymmetric shear-layer calculation are given by

$$\beta_1 = \int_0^\infty gf(f-R)\,d\eta$$

$$\beta_2 = \int_0^\infty gf(f-R)\eta\,d\eta$$

$$\beta_3 = \int_0^\infty gf(f^2-R^2)\,d\eta$$

$$\beta_4 = \int_0^\infty gf(f^2-R^2)\eta\,d\eta$$

$$k_1 = \frac{1}{2}\int_0^\infty g\,\Re[\hat{\omega}\hat{u}^*]\frac{df}{d\eta}\,d\eta$$

$$k_2 = \frac{1}{2}\int_0^\infty g\,\Re[\hat{\omega}\hat{u}^*]\frac{df}{d\eta}\eta\,d\eta$$

$$k_3 = 2b(C_1 - C_2\beta_1) + C_2\left(C_3 + \frac{C_4}{C_3}\right)$$

where

$$C_1 = \beta_4 - (1+R)\beta_2$$

$$C_2 = \frac{[\beta_3 - (1+R)\beta_1]}{(1-R)}$$

$$C_3 = \sqrt{b^2\beta_1^2 - (1-R)(2b^2\beta_2 - 1 + R)}$$

$$C_4 = b^2[\beta_1^2 - 2(1-R)\beta_2]$$

The integrals and coefficients required for the two-dimensional shear-layer calculation are given by

$$k_4 = (1-R)^2[RI_3 + (1-R)I_4]$$

where

$$I_3 = \int_{-\infty}^\infty gf(1-f)\,d\eta$$

$$I_4 = \int_{-\infty}^\infty gf^2(1-f)\,d\eta$$

Acknowledgments

This work was supported by the Office of Naval Research and the Air Force Office of Scientific Research under Grant N00014-88-K-0242. The technical monitors were S. G. Lekoudis and J. Tishkoff.

References

[1]Brown, G. L., and Roskho, A., "On Density Effects and Large Structures in Turbulent Mixing Layers," *Journal of Fluid Mechanics,* Vol. 64, Pt. 4, 1974, pp. 775–816.

[2]Hussain, A. K. M. F., "Coherent Structures and Turbulence," *Journal of Fluid Mechanics,* Vol. 173, Dec. 1986, pp. 303–356.

[3]Gaster, M., Kit, E., and Wygnanski, I., "Large-Scale Structures in a Forced Turbulent Mixing Layer," *Journal of Fluid Mechanics,* Vol. 150, Jan. 1985, pp. 23–39.

[4]Petersen, R. A., and Samet, M. M., "On the Preferred Mode of Jet Instability," *Journal of Fluid Mechanics,* Vol. 194, Sept. 1988, pp. 153–173.

[5]Lepicovsky, J., Ahuja, K. K., Brown, W. H., and Burrin, R. H., "Coherent Large-Scale Structures in High Reynolds Number Supersonic Jets," NASA CR-3952, 1985.

[6]Papamoschou, D., and Roshko, A., "The Compressible Turbulent Shear Layer: An Experimental Study," *Journal of Fluid Mechanics,* Vol. 197, Dec. 1988, pp. 453–477.

[7]Morris, P. J., and Tam C. K. W., "On the Radiation of Sound by Instability Waves of a Compressible Axisymmetric Jet," *Mechanics of Sound Generation in Flows,* edited by E. A. Muller, Springer-Verlag, 1979, pp. 55–61.

[8]Tam, C. K. W., and Burton, D. E., "Sound Generated by Instability Waves of Supersonic Flows. Part 2. Axisymmetric Jets," *Journal of Fluid Mechanics,* Vol. 138, Jan. 1984, pp. 273–295.

[9]Tam, C. K. W., and Morris, P. J., "Tone Excited Jets, Part V: A Theoretical Model and Comparison with Experiments," *Journal of Sound and Vibration,* Vol. 102, Pt. 1, 1985, pp. 119–151.

[10]Morris, P. J., Giridharan, M. G., and Lilley, G. M., "On the Turbulent Mixing of Compressible Free Shear Layers," *Proceedings of the Royal Society of London, Series A: Mathematical and Physical Sciences,* Vol. 431, 1990, pp. 219–243.

[11]Ho, C. M., and Huang, L. S., "Subharmonics and Vortex Merging in Mixing Layers," *Journal of Fluid Mechanics,* Vol. 119, Jan. 1982, pp. 443–473.

[12]Zhuang, M., Kubota, T., and Dimotakis, P. E., "On the Instability of Inviscid, Compressible Free Shear Layers," AIAA Paper 88-3538, 1988.

[13]Sandham, N., and Reynolds, W. C., "Compressible Mixing Layer: Linear Theory and Direct Simulation," *AIAA Journal,* Vol. 28, 1990, pp. 618–624.

[14]Ragab, S. A., and Wu, J. L., "Linear Instability Waves in Supersonic Turbulent Mixing Layers," *AIAA Journal,* Vol. 27, 1989, pp. 677–686.

[15]Morkovin, M. V., "Effects of Compressibility on Turbulent Flows," *The Mechanics of Turbulence,* edited by A. Favre, Gordon and Beach, New York, 1964, pp. 367–379.

[16]Bradshaw, P., "Compressible Turbulent Shear Layers," *Annual Review of Fluid Mechanics,* Vol. 9, 1977, pp. 33–54.

[17]Morkovin, M. V., "Mach Number Effects on Free and Wall Turbulent Structures in Light of Instability Flow Interactions," *Recent Developments in Turbulence: The Lumley Symposium,* edited by T. B. Gatski, S. Sarkar, and C. G. Speziale, Springer-Verlag, 1991.

[18]Tam, C. K. W., and Morris, P. J., "The Radiation of Sound by the Instability Waves of a Compressible Plane Turbulent Shear Layer," *Journal of Fluid Mechanics,* Vol. 98, Pt. 2, 1980, pp. 349–381.

[19]Bogdanoff, D. W., "Compressibility Effects in Turbulent Shear Layers," *AIAA Journal,* Vol. 21, No. 6, 1983, pp. 926,927.

[20]Papamoschou, D., "Structure of the Compressible Shear Layer," AIAA Paper 90-0126, Jan. 1989.

[21]Messersmith, N. L., Goebel, S. G., Frantz, W. H., Krammer, E. A., Renie, J. P., Dutton, J. C., and Krier, H., "Experimental and Analytical Investigations of Supersonic Mixing Layers," AIAA Paper 88-0702, Jan. 1988.

[22]Giridharan, M. G., and Morris, P. J., "The Development of Wave Packets in Supersonic Shear Layers," AIAA Paper 91-0626, Jan. 1991.

[23]Morris, P. J., "Turbulence Measurements in Subsonic and Supersonic Axisymmetric Jets in a Parallel Stream," *AIAA Journal,* Vol. 14, 1976, pp. 1468–1475.

[24]Gutmark, E., Schadow, K. J., and Wilson, K. J., "Mixing Enhancement in Coaxial Supersonic Jets," AIAA Paper 89-1812, June 1989.

[25]Sarkar, S., Erlebacher, G., Hussaini, M. Y., and Kreiss, H. O., "The Analysis and Modeling of Dilatational Terms in Compressible Turbulence," Inst. for Computer Applications in Science and Engineering, Hampton, VA, Rept. 89-79, 1989.

[26]Sarkar, S., and Balakrishnan, L., "Application of a Reynolds Stress Turbulence Model to the Compressible Shear Layer," AIAA Paper 90-1465, June 1990.

[27]Erlebacher, G., Hussaini, M. Y., Kriess, H. O., and Sarkar, S., "The Analysis and Simulation of Compressible Turbulence," *Theoretical and Computational Fluid Dynamics,* Vol. 2, 1990, pp. 73–95.

[28]Liou, W. W., and Morris, P. J., "Wave Models for Turbulent Free Shear Flows," *Proceedings of the Symposium on Aeropropulsion,* NASA Lewis Research Center, April 1990, pp. 457–471.

[29]Chinzei, N., Masuya, G., Komuro, T., Murakami, A., and Kudou, K., "Spreading of Two-Stream Supersonic Turbulent Mixing Layers," *Physics of Fluids,* Vol. 29, No. 5, 1986, pp. 1345–1347.